

# Bimetallic Carbide Nanocomposite Enhanced Pt Catalyst with High Activity and Stability for the Oxygen Reduction Reaction

Xueming Ma,<sup>†</sup> Hui Meng,<sup>†</sup> Mei Cai,<sup>‡</sup> and Pei Kang Shen<sup>\*†</sup>

<sup>†</sup>State Key Laboratory of Optoelectronic Materials and Technologies and Key Laboratory of Low-Carbon Chemistry & Energy Conservation of Guangdong Province, School of Physics and Engineering, Sun Yat-sen University, 135 Xingang Road, Guangzhou 510275, P. R. China

<sup>‡</sup>General Motors Research and Development Center, Warren, Michigan 48090-9055, United States

## S Supporting Information

**ABSTRACT:** Nanocomposites consisting of the bimetallic carbide  $\text{Co}_6\text{Mo}_6\text{C}_2$  supported on graphitic carbon ( $^{\text{g}}\text{C}$ ) were synthesized in situ by an anion-exchange method for the first time. The  $\text{Co}_6\text{Mo}_6\text{C}_2/^{\text{g}}\text{C}$  nanocomposites were not only chemically stable but also electrochemically stable. The catalyst prepared by loading Pt nanoparticles onto  $\text{Co}_6\text{Mo}_6\text{C}_2/^{\text{g}}\text{C}$  was evaluated for the oxygen reduction reaction in acidic solution and showed superior activity and stability in comparison with commercial Pt/C. The higher mass activity of the Pt- $\text{Co}_6\text{Mo}_6\text{C}_2/^{\text{g}}\text{C}$  catalyst indicated that less Pt would be required for the same performance, which in turn would reduce the cost of the fuel cell electrocatalyst. The method reported here will promote broader interest in the further development of other nanostructured materials for real-world applications.

Platinum usage reduction is a critical challenge for the commercialization of fuel cell vehicles because of its high price and limited availability. An effective method for reducing Pt usage is to alloy Pt with other metal(s) to enhance the reactivity based on the ensemble, ligand, and geometric effects.<sup>1</sup> With this method, the amount of Pt can be reduced by more than 80% through the use of a dealloyed Pt core-shell-structured catalyst.<sup>1</sup> An alternative approach is to find proper supports that can promote the reactivity of Pt-based catalysts via synergistic effects.<sup>2</sup> Carbide-based electrocatalysts have been intensively studied because of their electrocatalytic synergistic effect and their Pt-like behavior for chemical catalysis.<sup>3</sup> It has been reported that carbide-based electrocatalysts are highly active for both the oxygen reduction reaction (ORR) and alcohol oxidation. However, a crucial problem that remains unsolved is the stability of the carbides.<sup>4</sup>

The present study attempts to explore a new way to stabilize carbide-based materials through the synthesis of bimetallic carbide nanocomposites. Relative to the traditional method for preparing carbides, which requires high energy consumption (high temperature), our method employs a much lower temperature by introducing an ion-exchange resin as the initial precursor. The preparation procedures include ion exchange with targeted ions followed by heat treatment. In this work, we report the synthesis of a nanocomposite of  $\text{Co}_6\text{Mo}_6\text{C}_2$  on graphitized carbon ( $^{\text{g}}\text{C}$ ) using an ion-exchange method. The

resulting product was further loaded with Pt nanoparticles and tested as an electrocatalyst (denoted as Pt- $\text{Co}_6\text{Mo}_6\text{C}_2/^{\text{g}}\text{C}$ ) for the ORR.

In a typical preparation, the pretreated resin was washed with deionized water and dried at 80 °C. Ten grams of macroporous acrylic-type anion-exchange resin (D314) was first impregnated with 100 mL of 0.1 mol L<sup>-1</sup>  $(\text{NH}_3)_6\text{Mo}_7\text{O}_{24}$  solution. The resin- $\text{Mo}_7\text{O}_{24}^{6-}$  complex was then impregnated again with 100 mL of 0.05 mol L<sup>-1</sup>  $\text{Na}_3\text{Co}(\text{NO}_2)_6$  solution. The resulting resin- $\text{Co}(\text{NO}_2)_6^{3-}/\text{Mo}_7\text{O}_{24}^{6-}$  complex was dried at 80 °C for 12 h, and then carbonization and graphitization were performed in a tube furnace at 1400 °C for 1.5 h at a heating rate of 10 °C min<sup>-1</sup> under a pure N<sub>2</sub> flow. After the sample was slowly cooled to room temperature, the resulting product was ground into a powder and treated with 5 mol L<sup>-1</sup> HCl solution to remove impurities. The  $\text{Co}_6\text{Mo}_6\text{C}_2/^{\text{g}}\text{C}$  sample was finally washed and dried before testing of its stability in acidic solution. The Pt- $\text{Co}_6\text{Mo}_6\text{C}_2/^{\text{g}}\text{C}$  electrocatalyst was then prepared by the intermittent microwave heating (IMH) method.<sup>5</sup>

X-ray diffraction (XRD), Raman spectroscopy, scanning electron microscopy (SEM), and transmission electron microscopy (TEM) were used for characterization. Electrochemical measurements were conducted on a PINE instrument in a three-electrode cell. The ORR testing was performed in an oxygen-saturated 0.1 mol L<sup>-1</sup> HClO<sub>4</sub> solution at 30 °C at a sweep rate of 5 mV s<sup>-1</sup> under a rotating speed of 1600 rpm.

Figure 1a displays the XRD pattern of a sample that was heat-treated at 1400 °C. As shown in the figure, pure  $\text{Co}_6\text{Mo}_6\text{C}_2$  on graphitized carbon can be formed at 1400 °C. Below 1400 °C, the bimetallic carbide could hardly be formed (Figure S1 in the Supporting Information), and the dominant products were found to be Mo<sub>2</sub>C and Co. The degree of graphitization can be calculated from the relative intensities of the D and G bands in the Raman spectrum (Figure S2). The two peaks at 1356 and 1584 cm<sup>-1</sup> are ascribed to the asymmetry breakdown at the edge of graphene sheets (D band) and the E<sub>2g</sub> vibrational mode of the graphite layers (G band), respectively.<sup>6</sup> The I<sub>G</sub>/I<sub>D</sub> ratio is 2.97, suggesting an extremely high degree of graphitization. This result is in good agreement with the XRD results, where the distinct graphite diffraction peak at 2θ = 26.23° was observed.

Received: November 2, 2011

Published: January 20, 2012

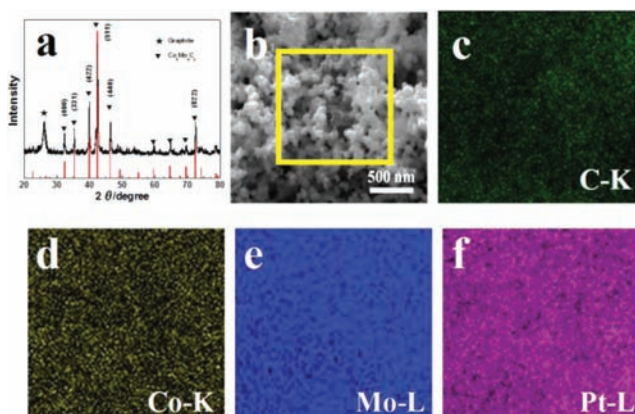


**Figure 1.** (a) XRD pattern of  $\text{Co}_6\text{Mo}_6\text{C}_2/\text{gC}$ . (b) SEM micrograph and (c–f) elemental mapping images of Pt– $\text{Co}_6\text{Mo}_6\text{C}_2/\text{gC}$ .

The Pt nanoparticles were loaded onto the  $\text{Co}_6\text{Mo}_6\text{C}_2/\text{gC}$  nanocomposite by IMH-assisted ethylene glycol reduction.<sup>2a,3b</sup> Figure S3 shows the XRD pattern of Pt– $\text{Co}_6\text{Mo}_6\text{C}_2/\text{gC}$ . The peaks at  $2\theta = 39.76$ ,  $46.24$ , and  $67.71^\circ$  are indexed as the (111), (200), and (220) planes, respectively, of face-centered-cubic Pt, confirming the formation of Pt nanoparticles. The particle size was 4.3 nm, as calculated by the Scherrer equation.

Figure 1b is an SEM micrograph of the as-prepared Pt– $\text{Co}_6\text{Mo}_6\text{C}_2/\text{gC}$  sample. It shows a uniform distribution of  $\text{Co}_6\text{Mo}_6\text{C}_2$  particles. Figure S4 is the energy-dispersive X-ray spectrum (EDS) of Pt– $\text{Co}_6\text{Mo}_6\text{C}_2/\text{gC}$ , which proves the coexistence of Pt, Co, Mo, and C in the product. Figure 1c–f shows the elemental dispersion of C, Co, Mo, and Pt in Pt– $\text{Co}_6\text{Mo}_6\text{C}_2/\text{gC}$ . The four elements in the product were uniformly distributed in the randomly selected area.

The  $\text{gC}$  produced in this work was cage-structured and highly graphitized, as shown in Figure 2a,b. Figure 2a shows that the

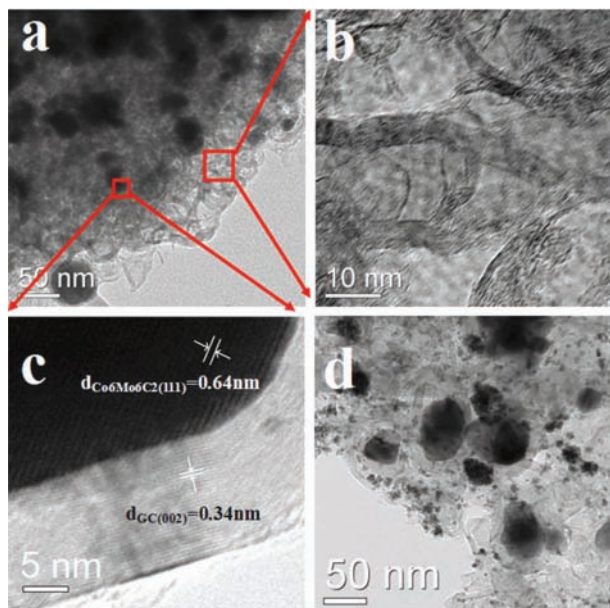


**Figure 2.** (a) TEM image of  $\text{Co}_6\text{Mo}_6\text{C}_2/\text{gC}$ , (b) HRTEM image of  $\text{gC}$ , (c) HRTEM image of  $\text{Co}_6\text{Mo}_6\text{C}_2/\text{gC}$ , and (d) TEM image of Pt– $\text{Co}_6\text{Mo}_6\text{C}_2/\text{gC}$ .

$\text{Co}_6\text{Mo}_6\text{C}_2$  nanoparticles were well-dispersed in the composite with a narrow particle size. The average size of the

nanoparticles was  $\sim 50$  nm. It is difficult to prepare  $\text{Co}_6\text{Mo}_6\text{C}_2$  nanoparticles smaller than 50 nm at the moment. The optimization of experimental conditions, which is in progress, may lead to a  $\text{Co}_6\text{Mo}_6\text{C}_2$  product with sizes of 10 nm or less. The  $\text{Co}_6\text{Mo}_6\text{C}_2$  nanoparticles were partially buried in the  $\text{gC}$  as a stable support for loading of Pt nanoparticles. The well-defined crystal fringes in the high-resolution TEM (HRTEM) images in Figure 2b,c proved the graphitic nature of the carbon. The formation of  $\text{gC}$  cages was most probably due to gas evolution during the evaporation and decomposition of the resin before graphitization. The  $\text{gC}$  cages were connected with each other, enhancing the electrical conductivity of the support. The TEM image in Figure 2d shows that the Pt nanoparticles were uniformly dispersed on the  $\text{gC}$  and  $\text{Co}_6\text{Mo}_6\text{C}_2$  particles.

Figure 3 compares the ORR performances of the Pt/C and Pt– $\text{Co}_6\text{Mo}_6\text{C}_2/\text{gC}$  catalysts in  $\text{O}_2$ -saturated  $0.1 \text{ mol L}^{-1} \text{ HClO}_4$

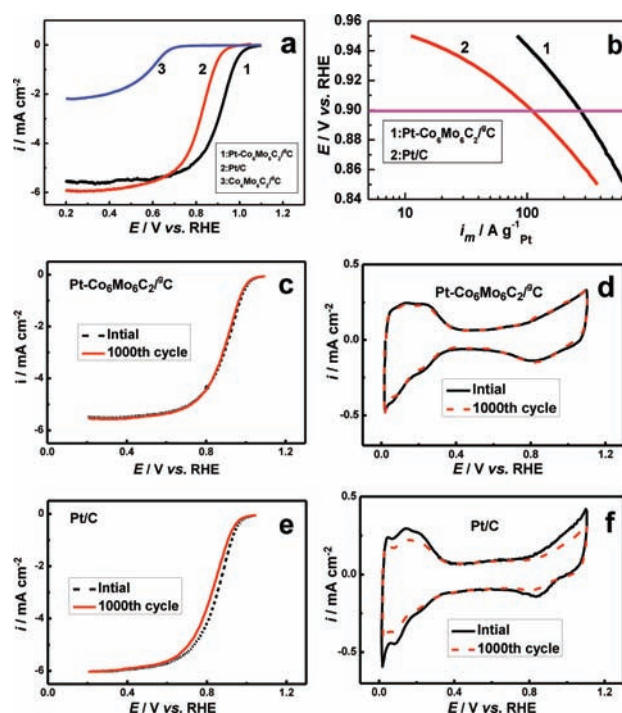


**Figure 3.** (a) Linear potential sweep curves for the ORR on Pt/C,  $\text{Co}_6\text{Mo}_6\text{C}_2/\text{gC}$ , and Pt– $\text{Co}_6\text{Mo}_6\text{C}_2/\text{gC}$ . (b) Mass activities for the ORR on two different catalysts. (c, e) ORR curves before and after 1000 cycles on (c) Pt– $\text{Co}_6\text{Mo}_6\text{C}_2/\text{gC}$  and (e) Pt/C catalysts. (d, f) CVs before and after 1000 cycles on (d) Pt– $\text{Co}_6\text{Mo}_6\text{C}_2/\text{gC}$  and (f) Pt/C in background solution.

aqueous solution at 1600 rpm and a potential sweep rate of  $5 \text{ mV s}^{-1}$  at  $30^\circ \text{C}$ .  $\text{Co}_6\text{Mo}_6\text{C}_2/\text{gC}$  alone is active for the ORR, but the overpotential is very high relative to that of Pt– $\text{Co}_6\text{Mo}_6\text{C}_2/\text{gC}$  under the same conditions (trace 3 in Figure 3a). The Pt– $\text{Co}_6\text{Mo}_6\text{C}_2/\text{gC}$  catalyst exhibited superior ORR activity in comparison with Pt/C and  $\text{Co}_6\text{Mo}_6\text{C}_2/\text{gC}$ . The half-wave potential of the ORR on Pt– $\text{Co}_6\text{Mo}_6\text{C}_2/\text{gC}$  was 80 mV more positive than that on the Pt/C catalyst, indicating that the introduction of  $\text{Co}_6\text{Mo}_6\text{C}_2/\text{gC}$  to the Pt catalyst significantly improved the ORR kinetics by lowering the overpotential. The positive shift of 80 mV for the ORR is of great value in fuel cells, since the reasonable voltage output for a single  $\text{H}_2/\text{O}_2$  fuel cell is 0.6–0.7 V.<sup>7</sup> The high performance of the Pt–

$\text{Co}_6\text{Mo}_6\text{C}_2/\text{C}$  catalyst can be explained by the synergistic effect between the  $\text{Co}_6\text{Mo}_6\text{C}_2$  support and the active Pt metal. The origin of the synergistic effect can be explained by our previous work,<sup>8</sup> which showed that tungsten carbide (WC) had a synergistic effect with Pt in both methanol oxidation and the ORR. The synergistic effect was explained by the strong negative electronic property of WC: when WC was used as the support for Pt to form the Pt–WC/C catalyst, the surface electronic structure of Pt–WC/C was very different from that of the Pt/C catalyst as a result of the electron-donating effect generated by the WC support. Thus, Pt–WC/C showed an obvious anti-CO-poisoning effect in the electrooxidation of methanol. Since  $\text{Co}_6\text{Mo}_6\text{C}_2$  is also a carbide and Mo belongs to the same group as W, the same electron-donating effect may also exist with  $\text{Co}_6\text{Mo}_6\text{C}_2$ , resulting in the change of the surface electronic structure of Pt. This may be the origin of the enhancement of the ORR performance of the Pt– $\text{Co}_6\text{Mo}_6\text{C}_2/\text{C}$  catalyst.

The Pt mass activity on Pt/C was  $108.6 \text{ A g}_{\text{Pt}}^{-1}$  in this work, while the Pt– $\text{Co}_6\text{Mo}_6\text{C}_2/\text{C}$  catalyst showed a mass activity of  $271.7 \text{ A g}_{\text{Pt}}^{-1}$  at 0.9 V (Table 1), which is 2.5 times higher than

**Table 1. ORR Parameters of Pt/C and Pt– $\text{Co}_6\text{Mo}_6\text{C}_2/\text{C}$**

catalyst	$E_{\text{onset}}$ (V)	$E_{1/2}$ (V)	$i_{\text{m}(0.9 \text{ V})}$ ( $\text{A g}_{\text{Pt}}^{-1}$ )
40%Pt/C	0.98	0.84	108.6
40%Pt– $\text{Co}_6\text{Mo}_6\text{C}_2/\text{C}$	1.06	0.92	271.7

that of Pt/C. The hydrogen peroxide yields of these catalysts were also calculated and compared. The results (Figure S5b) indicate that the percentage of  $\text{H}_2\text{O}_2$  generated on the Pt– $\text{Co}_6\text{Mo}_6\text{C}_2/\text{C}$  catalyst was almost half of that of the Pt/C catalyst in the whole potential range, which further proves the higher ORR activity of the Pt– $\text{Co}_6\text{Mo}_6\text{C}_2/\text{C}$  catalyst relative to the Pt/C catalyst.

The stability is one of the critical factors for a practical fuel cell catalyst. To evaluate the stability of the Pt– $\text{Co}_6\text{Mo}_6\text{C}_2/\text{C}$  catalyst, comparisons of the ORR polarization curves and corresponding cyclic voltammograms (CVs) for Pt– $\text{Co}_6\text{Mo}_6\text{C}_2/\text{C}$  and Pt/C before and after 1000 cycles were carried out in oxygen-saturated 0.1 mol  $\text{L}^{-1}$   $\text{HClO}_4$  solution at 30 °C (Figure 3c–f). The potential range was 0.05–1.1 V vs RHE, and the scan rate was 50  $\text{mV s}^{-1}$ . After 1000 cycles, there was only a 6 mV degradation in the half-wave potential on Pt– $\text{Co}_6\text{Mo}_6\text{C}_2/\text{C}$  (Figure 3c), while the corresponding potential for Pt/C decreased by 27 mV (Figure 3e). This is direct evidence of the better stability of Pt– $\text{Co}_6\text{Mo}_6\text{C}_2/\text{C}$  in comparison with Pt/C. The corresponding losses of the active surface areas are shown in Figure 3d,f. Upon integration of the charge between 0 and 0.36 V associated with hydrogen adsorption, no recordable loss of surface area on Pt– $\text{Co}_6\text{Mo}_6\text{C}_2/\text{C}$  was observed, while ~20% loss of surface area on Pt/C was observed. The improved stability might originate from  $\text{Co}_6\text{Mo}_6\text{C}_2/\text{C}$ , which is much more stable than carbon under the testing conditions.<sup>9</sup>

In summary,  $\text{Co}_6\text{Mo}_6\text{C}_2/\text{C}$  nanocomposites were prepared for the first time by an in situ ion-exchange method. The physical characterization proved that the  $\text{Co}_6\text{Mo}_6\text{C}_2$  was uniformly dispersed on graphitized carbon with an average particle size of 50 nm. The  $\text{Co}_6\text{Mo}_6\text{C}_2/\text{C}$  nanocomposite was further used as a catalyst support for loading of Pt nanoparticles for ORR testing in acidic solution, and the resulting Pt– $\text{Co}_6\text{Mo}_6\text{C}_2/\text{C}$  catalyst showed superior activity and stability in

comparison with Pt/C. The higher mass activity of Pt– $\text{Co}_6\text{Mo}_6\text{C}_2/\text{C}$  indicated that less Pt would be required for the same performance, which would in turn reduce the cost of the fuel cell. The novelty of this work is not only the fundamental understanding and scientific discovery of new nanomaterials but also its readiness for large-scale production and industrial application.

## ■ ASSOCIATED CONTENT

### ● Supporting Information

Synthesis details and additional physical characterization. This material is available free of charge via the Internet at <http://pubs.acs.org>.

## ■ AUTHOR INFORMATION

### Corresponding Author

stsspk@mail.sysu.edu.cn

### Notes

The authors declare no competing financial interest.

## ■ ACKNOWLEDGMENTS

This work was supported by the National Natural Science Foundation of China (U1034003, 21073241, 21106190), the China National 863 Program (2009AA034400), the State Key Laboratory of Optoelectronic Materials and Technologies (2010-ZY-4-4, 2010-ZY-4-7), and General Motors (Project RD-07-295-NV508). H.M. thanks the Doctoral Fund of the Ministry of Education of China (20100171120022).

## ■ REFERENCES

- (1) (a) Maroun, F.; Ozanam, F.; Magnussen, O. M.; Behm, R. J. *Science* **2001**, *293*, 1811–1814. (b) Chen, M.; Kumar, D.; Yi, C. W.; Goodman, D. W. *Science* **2005**, *310*, 291–293. (c) Stamenkovic, V. R.; Fowler, B.; Mun, B. S.; Wang, G.; Ross, P. N.; Lucas, C. A.; Marković, N. M. *Science* **2007**, *315*, 493–497. (d) Mazumder, V.; Chi, M.; More, K. L.; Sun, S. H. *J. Am. Chem. Soc.* **2010**, *132*, 7848–7849. (e) Wang, D.; Xin, H. L.; Yu, Y.; Wang, H.; Rus, E.; Muller, D. A.; Abruña, H. D. *J. Am. Chem. Soc.* **2010**, *132*, 17664–17666. (f) Zhou, Y.; Neyerlin, K.; Olson, T. S.; Pylypenko, S.; Bult, J.; Dinh, H. N.; Gennett, T.; Shao, Z.; O’Hayre, R. *Energy Environ. Sci.* **2010**, *3*, 1437–1446. (g) Strasser, P.; Koh, S.; Anniyev, T.; Greeley, J.; More, K.; Yu, C.; Liu, Z.; Kaya, S.; Nordlund, D.; Ogasawara, H.; Toney, M. F.; Nilsson, A. *Nat. Chem.* **2010**, *2*, 454–460.
- (2) (a) Meng, H.; Shen, P. K. *Chem. Commun.* **2005**, 4408–4410. (b) Pang, M.; Li, C.; Ding, L.; Zhang, J.; Su, D.; Li, W.; Liang, C. *Ind. Eng. Chem. Res.* **2010**, *49*, 4169–4174. (c) Joo, S. H.; Choi, S. J.; Oh, I.; Kwak, J.; Liu, Z.; Terasaki, O.; Ryoo, R. *Nature* **2001**, *412*, 169–172.
- (3) (a) Meng, H.; Shen, P. K. *J. Phys. Chem. B* **2005**, *109*, 22705–22709. (b) Yin, S. B.; Cai, M.; Wang, C. X.; Shen, P. K. *Energy Environ. Sci.* **2011**, *4*, 558–563. (c) Levy, R. B.; Boudart, M. *Science* **1973**, *181*, 547–549.
- (4) (a) Ganesan, R.; Lee, J. S. *Angew. Chem., Int. Ed.* **2005**, *44*, 6557–6560. (b) Bodoardo, S.; Maja, M.; Penazzi, N.; Henn, F. E. G. *Electrochim. Acta* **1997**, *42*, 2603–2609. (c) Barnett, C. J.; Burstein, G. T.; Kucernak, A. R. J.; Williams, K. R. *Electrochim. Acta* **1997**, *42*, 2381–2388.
- (5) (a) Shen, P. K.; Tian, Z. Q. *Electrochim. Acta* **2004**, *49*, 3107–3111. (b) See the Supporting Information.
- (6) Obratsova, E. D.; Fujii, M.; Hayashi, S.; Kuznetsov, V. L.; Butenko, Y. V.; Chuvin, A. L. *Carbon* **1998**, *36*, 821–826.
- (7) Wang, Y.; Song, S.; Maragou, V.; Shen, P. K.; Tsiakaras, P. *Appl. Catal., B* **2009**, *89*, 223–228.
- (8) Cui, G. F.; Shen, P. K.; Meng, H.; Zhao, J.; Wu, G. J. *Power Sources* **2011**, *196*, 6125–6130.

(9) (a) Eastwood, B. J.; Christensen, P. A.; Armstrong, R. D.; Bates, N. R. J. *Solid State Electrochem.* **1999**, *3*, 179–186. (b) Yu, X.; Ye, S. J. *Power Sources* **2007**, *172*, 145–154.